Energy Proceedings
Vol 54, 2025
ISSN 2004-2965

Pore-Scale Heterogeneity and Salinity Impacts on CO_2 Storage in Deep Saline Aquifers: A Microfluidic and Computational Investigation[#]

Rajat Dehury, Jitendra S. Sangwai[*]
Department of Chemical Engineering, Indian Institute of Technology Madras,
Chennai, Tamil Nadu 600 036, India.
(Corresponding Author: jitendrasangwai@iitm.ac.in)

ABSTRACT

Achieving net-zero emissions and curbing the long-term increase in global warming requires large-scale carbon dioxide (CO_2) sequestration through various techniques. Among the plethora of options for large-scale CO_2 storage, geological storage stands out as the most promising, given its expansive storage capacity and minimal environmental impact. Deep saline aquifers, in particular, have emerged as frontrunners due to their vast storage potential and broad global availability. In saline aquifers, various trapping mechanisms, including structural and stratigraphic trapping, residual or capillary trapping, solubility trapping, and mineral trapping, work synergistically to store CO_2. The displacement dynamics of CO_2-brine two-phase flow in pore-scale dictates the structural and residual trapping of CO_2 in subsurface formations. In this regard, a highly heterogeneous porous microchannel was used to investigate the impact of salinity and porous heterogeneity on CO_2-brine displacement dynamics. A computational fluid dynamics (CFD) simulation based on the volume-of-fluid (VOF) method was used to study the immiscible two-phase flow dynamics under deep reservoir extreme temperature and pressure conditions. Microfluidic experiments, conducted under a high-resolution digital microscope with different brine salinities, provide pore-scale flow visualization and quantification of trapped CO_2. Meanwhile, CFD simulations on the same porous media consider thermophysical property changes for CO_2 and brine under high-pressure and high-temperature conditions, elucidating their impact on CO_2 trapping or storage. The observed unstable finger-like displacement pattern in the microchannel, attributed to very low capillary number (Ca) and viscosity ratio (M) values, results in CO_2 channeling with limited water displacement, thus restricting CO_2 saturation at around 50 %. Along with viscous fingering, small pore-throats pronounce the snap-off effects at the micro-scale, which increase the residual trapping of CO_2 in the porous media. An increase in brine salinity increases viscosity, interfacial tension, and contact angle, leading to a more vertical sweep of water and increasing the CO_2 storage capacity of a saline aquifer. Under reservoir conditions, the comparatively higher density of CO_2 and increase in contact angle resulting from the adsorption of CO_2 increases CO_2 trapping in porous channels. This combined approach of microfluidic experiments and CFD simulations provided valuable visualization and insights into CO_2-brine dynamics at the pore-scale, which would contribute significantly towards efficient, enhanced, and secure storage of CO_2.

Keywords: capillary number, CO_2 geo-sequestration, micromodel, porous media, saline aquifers, snap-off effect

NOMENCLATURE

Abbreviations	
CCUS	Carbon capture, utilization, and sequestration
CFD	*Computational fluid dynamics*
IEA	*International Energy Agency*
IFT	*Interfacial tension*
Gt	*Gigatons*
VOF	*Volume of fluid*
Symbols	
Ca	*Capillary number*
E	*Total mass-averaged energy*
$\vec{F}_{csf}$	*Interfacial force term*
h	*Enthalpy*
$\vec{J}$	*Total diffusive flux*
k	*Interface curvature*
K_{eff}	*Effective conductivity*
M	*Viscosity ratio*
$\hat{n}$	*Unit surface normal*
P	*Pressure*

This is a paper for the 16th International Conference on Applied Energy (ICAE2024), Sep. 1-5, 2024, Niigata, Japan.

t	*time*
T	*Temperature*
$\vec{v}$	*Velocity*
α	*Volume fraction*
μ	*Viscosity*
Σ	*Interfacial tension*
θ_w	*Contact angle*
P	*Density*
$\bar{\bar{\tau}}$	*Viscous stress tensor*

1. INTRODUCTION

According to the International Energy Agency (IEA), the world's energy supply is projected to increase by 21% by 2050 compared to 2022 under currently stated policy scenarios due to several factors, including economic growth, population growth, and technological advances [1]. As of 2023, fossil fuels still dominate the world energy sector, contributing to over 80 % of the world's total energy demand [2]. Annual carbon dioxide (CO_2) emissions also increased up to around 36.3 Gt/yr (gigatons per year) in 2021, with an average CO_2 level of 416 ppm in the atmosphere [3, 4]. Therefore, immediate actions must be taken to meet the Paris Agreement goal of limiting global temperature by 1.5°C and achieving net-zero scenarios. Various ways for transitioning to net-zero economies involve transitioning to renewable energy sources, improving the energy efficiency of different energy extensive processes, implementing large-scale carbon capture, utilization, and sequestration (CCUS) methods, improving policy and regulatory processes for climate change, and promoting international cooperation for clean technologies. Considering the dependence of the energy sector on fossil fuels, it is evident that other options like CCUS should be regarded rather than focusing only on renewable energy sources. After capturing carbon dioxide, it must be sequestered in underground geological formations or deep ocean waters.

Considering safety and environmental concerns for marine life, large capacities of underground porous media, monitoring accessibility, and public acceptance, geological storage seems to be the better option at this time [5]. Underground formations suitable for CO_2 sequestration can be either porous media like depleted oil and gas reservoirs and aquifers or non-porous media like host rocks, salt caverns, and abandoned mines. In porous media, gas is stored in interconnected pores or voids previously saturated with saline water or hydrocarbon fluids [6]. Along with depleted reservoirs, saline aquifers are also being explored by the scientific community for large-scale CO_2 storage due to their broader availability, versatility with depth and size, reduced leakage and environmental impact (due to mixing with the oil), and potential dual-purpose use as enhanced geothermal systems [7, 8]. There are four primary trapping mechanisms that aid in the safe storage of CO_2 in underground porous media such as structural/stratigraphical, residual, solubility, and mineral trapping [9]. All four trapping mechanisms contribute towards secure CO_2 sequestration in the case of subsurface saline aquifers.

An accurate assessment of CO_2-brine displacement dynamics in the pore scale determines the structural, solubility, and residual trapping of CO_2. However, limited pore-scale studies have discussed gas displacement dynamics and the corresponding trapping capacity of porous media in terms of both qualitative and quantitative analysis. Moreover, gas-liquid two-phase flow in porous media gets highly complex due to unstable displacement patterns, which are not well investigated. Experimental studies involving microfluidic investigation, 3D X-ray microtomography technique, numerical simulations like lattice Boltzmann method, volume of fluid (VOF) method, and pore-network modeling approach have been utilized by researchers for pore-scale characterization of CO_2 trapping and storage capacity estimation [10-17]. Zhang *et al.* conducted a microfluidic investigation and compared the displacement efficiency of nitrogen (N_2), hydrocarbon gas, and CO_2 for miscible and immiscible displacement cases. The discussion focuses on geological CO_2 utilization and storage based on enhanced oil recovery and concludes that CO_2 is better for oil production, especially in deep reservoirs with high pressure [10]. Al-Zaidi *et al.* and Moghadasi *et al.* used the X-ray microtomography technique to understand CO_2-brine displacement dynamics in core samples in terms of pressure behavior. The unstable displacement dynamics are highlighted in these research articles [11], [14]. Basirat *et al.* used a numerical modeling technique in a 2D microscopic heterogeneous model with the phase field method for interface calculations between CO_2 and brine for deep investigation of underground carbon sequestration. The studies show that with a decrease in contact angle, the wetting phase (brine) saturation and normalized interfacial increases [12].

The microfluidic investigation provides a direct visualization during two-phase displacement experiments, allowing for the understanding of unstable displacement patterns like viscous and capillary fingering. In this study, both experimental and simulation techniques have been used to better understand the

displacement dynamics between CO_2 and brine. The same microfluidic model was used for both experimental and simulation studies, which mimics subsurface porous media. The study aims to quantify the structural and residual trapping of CO_2 and discuss the impact of pore heterogeneity and salinity on storage capacity.

2. MATERIALS AND METHODS

2.1 Numerical Methodology

To simulate CO_2-brine two-phase pore-scale flow, a computational fluid dynamics (CFD) simulation coupling with volume of fluid (VOF) method was used. The VOF model was used to track the interface between the two phases during the simulation. The VOF method introduced a new variable called volume fraction (α), and the corresponding continuity equation for α was solved for the interface tracking. Along with mass, momentum, and energy conservation principles, interfacial forces like viscous and capillary forces were introduced in the model to capture the unstable fingering phenomena at the pore scale. All the governing equations used in this simulation are shown in Table 1.

2.2 Porous Geometry and Experimental Setup

The porous media used for this study has a dimension of 20 mm × 10 mm × 20 µm, with 2.5D permeability and 0.57 porosity. For simulation purposes, a two-dimensional (2D) geometry was considered due to the small depth of the three-dimensional micromodel. The average pore size and throat size radii of the physical rock-type microchannel are 46 and 56 µm, respectively. The microfluidic device, as shown in Fig. 1a, has intricate and highly tortuous flow paths and mimics underground porous media. The microfluidic experiments to investigate CO_2-brine displacement dynamics were conducted under a digital microscope with a camera to capture the flow dynamics. Fig. 1b illustrates a simplified experimental setup with a syringe pump for CO_2/brine injection, a microchannel for flow experiments, a digital microscope and camera setup for flow visualization, and a computer for flow investigation. Five different salinities, 0, 10, 30, 60, and 80 parts per thousand (ppt) of water, were used to study the effect of salinity on two-phase displacement dynamics. Various salinity values were obtained from seawater (with approximately 30

Table 1 The governing equations used to simulate CO_2-brine two-phase immiscible flow in a heterogeneous porous media under subsurface reservoir conditions.

Equation Names	***Mathematical Representation***		***References***
Volume fraction tracking	$\frac{\partial}{\partial t}(\rho_1\alpha_1) + \nabla .(\rho_1\alpha_1\vec{v}) = 0$	(1)	[18, 19]
Navier-Stokes equations	$\frac{\partial}{\partial t}(\rho\overrightarrow{v}) + \nabla .(\rho\vec{v}\vec{v}) = -\nabla p + \nabla .[\mu(\nabla\vec{v} + \nabla\vec{v}^T)] + \vec{F}_{csf}$	(2)	[19, 20]
Surface force and wall adhesion term	$\vec{F}_{csf} = \sigma\frac{\rho k\nabla\alpha_1}{\frac{1}{2}(\rho_1+\rho_2)}$	(3)	[21, 22]
	$k = -(\nabla.\hat{n})$	(4)	
	$\hat{n} = \hat{n}_w cos\theta_w + \hat{t}_w sin\theta_w$	(5)	
Energy equation	$\frac{\partial}{\partial t}(\rho E) + \nabla \cdot \left(\vec{v}(\rho E + p)\right) = \nabla \cdot (K_{eff}\nabla T - \Sigma\Sigma\ h_{j,1}\vec{J}_{j,1} + (\bar{\bar{\tau}}\cdot\vec{v}))$	(6)	[19, 20]
Properties at the interface	$\rho = \alpha_1\rho_1 + (1-\alpha_1)\rho_2$	(7)	[18]
	$\mu = \alpha_1\mu_1 + (1-\alpha_1)\mu_2$	(8)	

ppt), either by diluting with distilled water or by evaporating the seawater. The water phase was dyed using a blue color dye to differentiate the two phases easily during the flow displacement experiments. Initially, the micromodel was completely saturated with brine. Following the brine saturation, it was left undisturbed for 12–24 hours to achieve a more accurate approximation of subsurface aquifers. CO_2 was injected from one side of the microchip to observe the displacement dynamics between the two phases. For each salinity case, experiments were repeated 2-3 times, and average values of flow saturation were reported. After each experiment, the chip was cleaned with ethanol, alkali, and toluene to remove any impurities and previous saline waters.

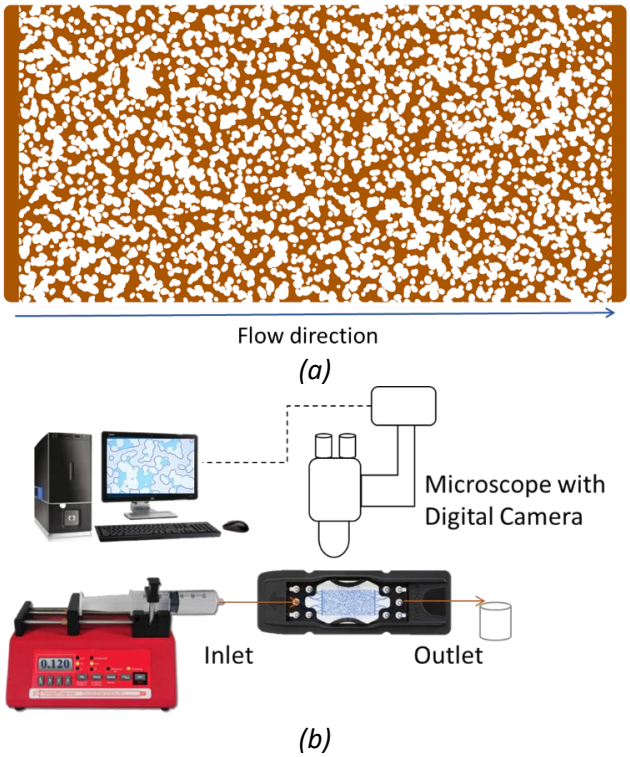

Fig. 1 (a) Heterogeneous porous media used for the two-phase flow investigation; (b) Experimental setup for microfluidic experiments.

2.3 Pore-scale Studies

All the microfluidic studies were carried out in atmospheric conditions, while numerical simulations were used to investigate under atmospheric and aquifer conditions (P = 15 MPa and T = 323 K). To understand the flow displacement regimes, all the simulation and experimental cases were plotted on a capillary number (*Ca*) vs. viscosity ratio (*M*) phase diagram, as shown in Fig. 2. *Ca* is defined as the ratio of the viscous force of injected fluid to capillary force ($Ca = \frac{\mu_2 u}{\sigma}$) and M is the ratio of viscous force between displacing and displaced fluid ($M = \frac{\mu_2}{\mu_1}$). All the considered cases lie between the viscous and capillary fingering regions, which allows to study the influence of viscous and capillary forces on displacement dynamics at the pore scale. The displacement regimes are divided following the works of Lenormand et al. and Zhang et al. [23, 24].

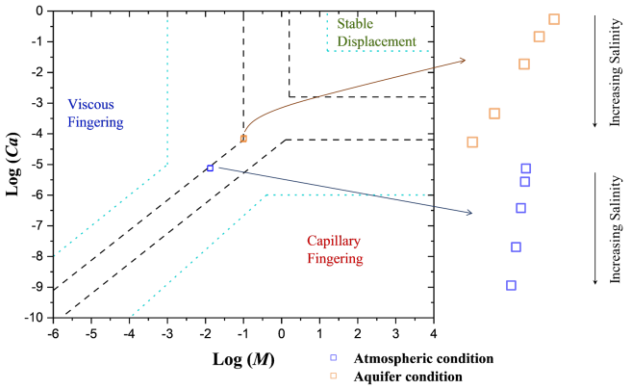

Fig.2 Log (Ca) vs. Log (M) phase diagram illustrating cases considered for this study and three different flow regimes following the work of references [23, 24].

Before carrying out the simulations discussed in this study, the CFD model was checked for mesh independence and validated by comparing it with microfluidic experiments. A detailed discussion on validation is available in our previous literature [20]. Along with atmospheric pressure, simulations were performed under high-pressure and high-temperature conditions observed in subsurface reservoirs. CO_2 becomes supercritical under these conditions, and its properties are calculated following the work of Span and Wagner [25]. The drastic change in CO_2 density and viscosity observed due to high pressure and temperature cases can be visualized in Fig. 3a and b. Brine and interfacial properties at these conditions were determined following previous literature [20, 26, 27].

3. RESULTS AND DISCUSSIONS

3.1 Experimental Observations

All the microfluidic experiments were conducted under atmospheric conditions to observe the brine displacement patterns and corresponding flow dynamics. The microfluidic device consists of multiple high-permeable, mid-permeable, low-permeable, and dead-end regions to mimic a physical rock found in subsurface saline reservoirs on a quasi-2D scale. A typical observation for a microfluidic experiment is

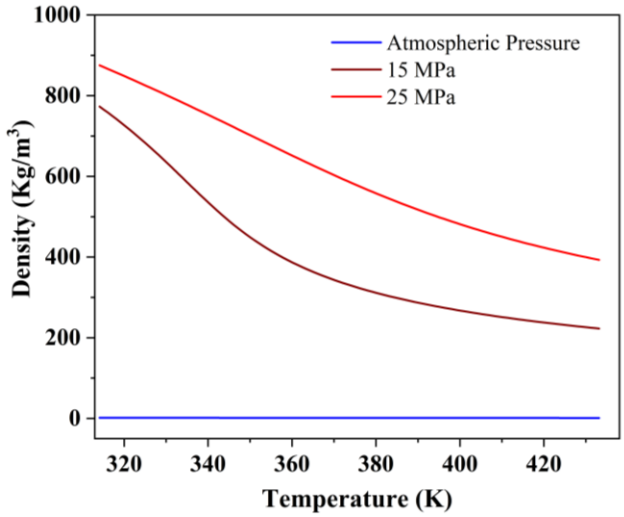

(a)

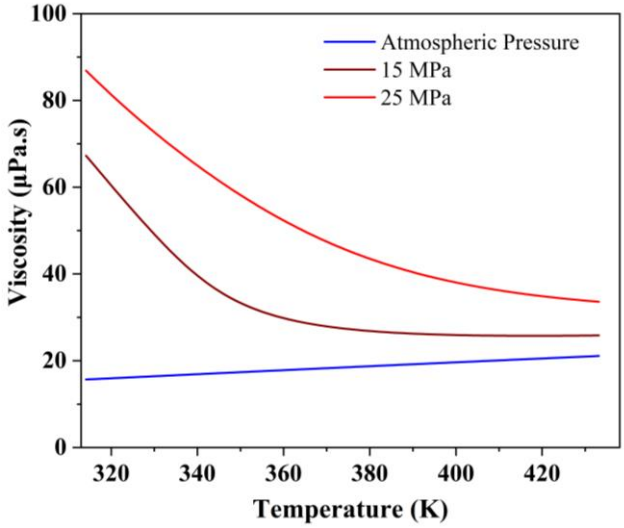

(b)

Fig. 3 Variation of CO_2 properties at high-pressure and high-temperature geological aquifer conditions (a) Density; (b) Viscosity.

demonstrated in Fig. 4a. Initially, a clean microchip was saturated with brine, and CO_2 was flooded. In atmospheric conditions, the interphase is clearly differentiable, indicating an immiscible phase displacement. To understand the physical displacement patterns at the pore scale, 8 locations on the microchip were identified with different permeabilities and at various distances from the injection side. Fig. 4b-d illustrates a few critical observations from the microfluidic experiments. CO_2 initially prefers a high-permeable flow path, creating multiple finger-like structures and channeling through these high-permeable channels (Fig. 4b and c). Viscous fingers developed due to the high viscosity contrast (M =0.01) between brine and CO_2, which can be observed throughout the micromodel. Fingers developed in the high-permeable path grow faster and create a positive feedback mechanism, allowing subsequent injected CO_2 to follow the same paths [20, 28]. Fingering patterns of mid and low-permeable flow paths only develop after the invasion of high-permeable micro channels (Fig. 4b). Fig. 4c illustrates the CO_2-channeling phenomena and poor sweep efficiency of dead-end regions. This CO_2 channeling through high-permeable channels limits the stratigraphical trapping of CO_2. The average CO_2 saturation observed for 10 ppt salinity brine invasion is 0.495. Fig. 4d shows the snapped-off CO_2 bubbles generated as the non-wetting phase separates from the continuous phase and moves separately.

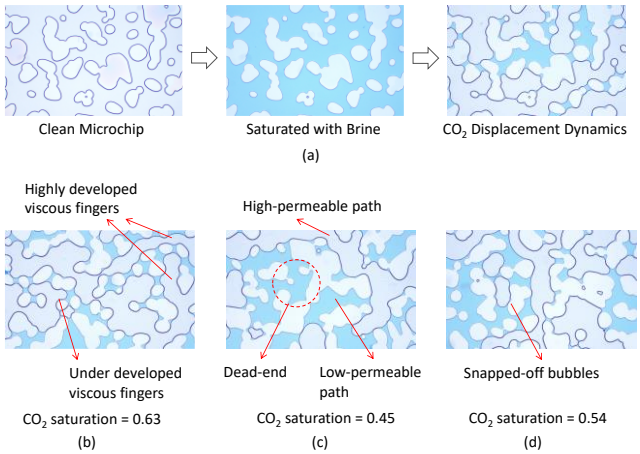

Fig. 4 Microfluidic experiments for the study of CO_2-brine (10 ppt) displacement dynamics. (a) A typical CO_2 flooding observation; (b) Different degrees of viscous fingering; (c) CO_2 channeling (d) CO_2 snap-off events.

3.2 Observations from CO_2 Pore-scale Simulations

CO_2-brine two-phase numerical simulations were carried out both at atmospheric and reservoir conditions. Under reservoir conditions, due to the supercritical nature of CO_2, breakthrough time and saturation at breakthrough increased significantly. The displacement patterns obtained from CFD simulations highlight the unstable nature of the brine invasion on a pore scale. For 10 ppt salinity values at the atmospheric conditions, Ca and M lie in the intermediate region between capillary and viscous fingering, and the corresponding displacement patterns are demonstrated in Fig. 5. The displacement patterns show unstable fingering patterns and snapped-off CO_2 bubbles. Snapped-off bubbles are generated when a gas bubble elongates while traveling through a narrow porous channel and gets disconnected from the continuous phase. A comprehensive understanding of the snap-off effect can help better

estimate CO_2 residual trapping inside a porous media. Higher degrees of snap-off events increase the residual trapping of CO_2 and may also increase the solubility trapping as the interfacial area between CO_2-brine increases with each snap-off event. Along with the channel geometry, the degree of snap-off events depends upon the flow rate of the injection, interfacial tension (IFT), and contact angle between rock-brine-CO_2. This study observed higher snap-off events for low-salinity brine, which can be attributed to their low contact angle and low IFT. The CO_2 breakthrough time for 10 ppt saline water is 0.739 s, and the CO2 saturation at breakthrough is 0.367. Microfluidic experiments generally estimate higher CO_2 saturation as these studies calculate saturation values after a steady state. However, in simulation cases, saturation values were obtained immediately after the breakthrough of CO_2 at the outlet. Comparing CO_2 saturation at breakthrough can be a better practice to have safe and efficient storage.

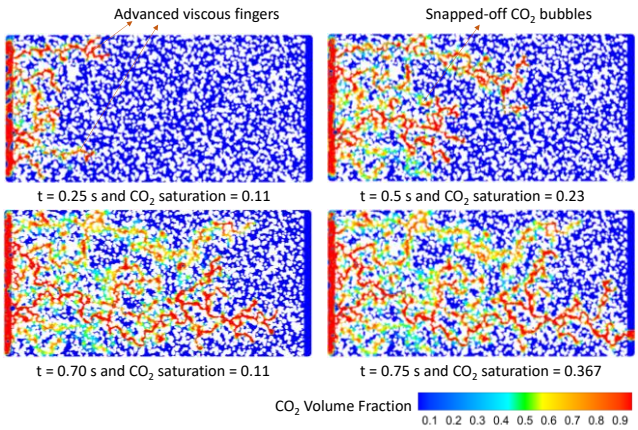

Fig. 5 Pore-scale displacement patterns at various time stages of CO_2-brine for 10 ppt salinity. Breakthrough time = 0.739 s and saturation at breakthrough = 0.367.

3.3 Impact of Salinity on CO_2 Trapping

Brine with five different salinity values, 0, 10, 30, 60, and 80 ppt, were used to investigate the impact of brine salinity on CO_2 trapping by stratigraphical and residual mechanisms and CO_2-brine displacement patterns. Simulations were conducted at atmospheric and high-pressure (P= 15 MPa) and high-temperature (T= 323 K) conditions. Fig. 6 shows a comparative plot of breakthrough time and saturation at breakthrough for different simulation cases. As illustrated with increased brine salinity, both breakthrough time and saturation increase. The trend is similar for both atmospheric and reservoir conditions. After 60 ppt salinity, CO_2 saturation remains constant, suggesting the influence of high viscous force dominating interfacial force compared to other salinity values. Even though the trend is similar for both atmospheric and aquifer conditions, the breakthrough time and CO_2 saturation increased by an average of 37.5 % and 29.1 % for underground aquifer conditions. The results show higher CO_2 storage capacity of high-temperature and high-pressure reservoirs due to the supercritical nature of CO_2. High density and high viscosity at reservoir conditions (Fig. 3) increased the time taken by CO_2 to reach the outlet of the micromodel.

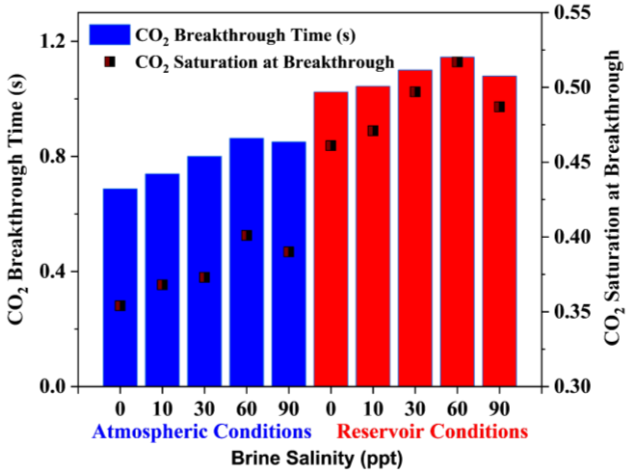

Fig. 6 CO_2 breakthrough time and CO_2 saturation at breakthrough for different salinity values both at atmospheric and geological reservoir conditions.

CO_2-brine displacement dynamics highly depend upon the interfacial forces, IFT, and contact angle. The variation of these two parameters determines the CO_2 storage capacity of the micromodel with varying salinity. Fig. 7a and b show the trend of IFT and contact angle for different salinity values at atmospheric and reservoir conditions. Both interfacial tension and contact angle increase with increased brine salinity for atmospheric and reservoir conditions. While in reservoir conditions, IFT decreases drastically, and the contact angle increases, making the system less water-wet. As a result, high-salinity brine is expected to displace easily, allowing more CO_2 storage capacity. Similar observations are obtained from the simulation results under extreme reservoir conditions.

4. CONCLUSION

CO_2 sequestrations will play a crucial role in achieving a net-zero economy. Subsurface saline aquifers have been explored as a potential site for large-scale, safe, and efficient carbon storage. In this context, this study explores the pore-scale flow dynamics of CO_2-brine, which helps understand CO_2 storage capacity and

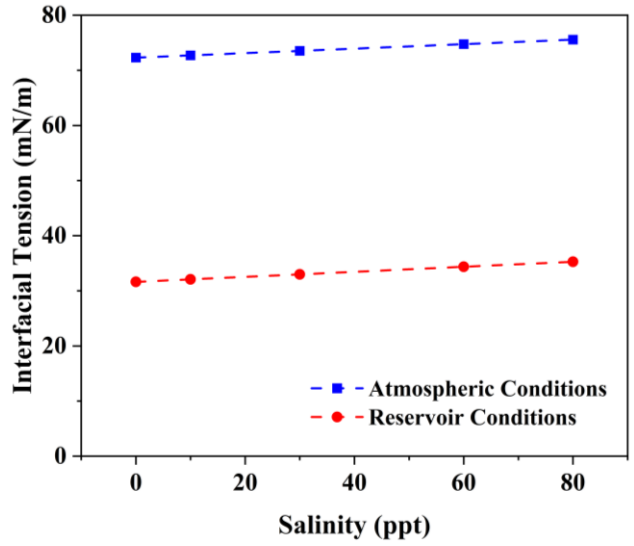

(a)

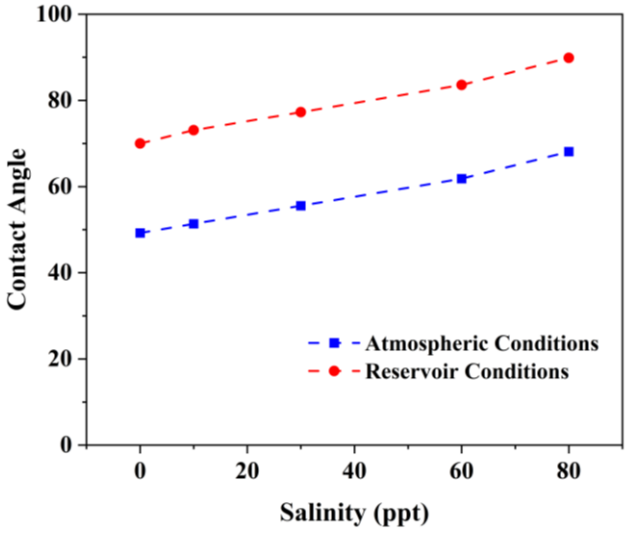

(b)

Fig. 7 (a) Interfacial tension and (b) Contact angle for different salinity values at atmospheric and reservoir conditions.

leakage status for a porous media filled with saline water. Five different salinity values, 0, 10, 30, 60, and 80 ppt, were considered to evaluate the impact of pore-scale heterogeneity and salinity on CO_2-brine two-phase flow in a heterogeneous porous microchannel. Microfluidic experiments were performed under atmospheric conditions, and numerical CFD simulations were conducted at atmospheric and high-pressure high-temperature conditions. Microfluidic experiments show the CO_2-brine displacement dynamics at various sections of the microchip. Degrees of viscous fingering, CO_2 channeling, and snap-off events characterize the CO_2-brine displacement dynamics at the pore scale. For reservoir conditions, CO_2 storage capacity increased by 29.1 % due to the high density and viscosity of supercritical CO_2. Storage capacity increases with the increase in salinity as the system becomes water-wet with higher salinity. Saline aquifers with a 30-60 ppt salinity can be used to get maximum storage capacity with a balance of viscous and capillary forces. Higher salinity also shifts the displacement dynamics slightly towards the capillary fingering regime. This combined approach of microfluidic experiments and CFD simulations provides a visualization of CO_2-brine two-phase displacement dynamics and helps predict the storage capacity of porous media, which would contribute towards a successful large-scale CO_2 sequestration.

REFERENCE

[1] IEA (2023), World Energy Outlook 2023, IEA, Paris https://www.iea.org/reports/world-energy-outlook-2023, Licence: CC BY 4.0 (report); CC BY NC SA 4.0 (Annex A).

[2] energyinst.org [internet]. 2024 Statistical Review of World Energy. c2024 [cited 2024 Oct 08]. Retrieved from: https://www.energyinst.org/statistical-review.

[3] Kumar Y, Sangwai JS. Environmentally Sustainable Large-Scale CO_2 Sequestration through Hydrates in Offshore Basins: Ab Initio Comprehensive Analysis of Subsea Parameters and Economic Perspective. Energ Fuel 2023;37(13):8739-8764. https://doi.org/10.1021/acs.energyfuels.3c00581.

[4] NOAA.gov [Internet]. Trends in Atmospheric Carbon Dioxide (CO_2); c2024 [cited 2024 Oct 08]. Retrieved from: https://gml.noaa.gov/ccgg/trends/global.html.

[5] Li Z, Dong M, Li S, Huang S. CO_2 sequestration in depleted oil and gas reservoirs-caprock characterization and storage capacity. Energy Convers Manag 2006;47(11–12):1372–1382. https://doi.org/10.1016/j.enconman.2005.08.023.

[6] Dehury R, Kumar Y, Sangwai JS. Methane storage underground. In: Rahimpour MR, Makarem MA, Meshksar M, editors. Advances and Technology Development in Greenhouse Gases: Emission, Capture and Conversion: Greenhouse Gases Storage and Transportation. Elsevier Inc. 2024, p. 251–273. https://doi.org/10.1016/B978-0-443-19067-4.00010-3.

[7] Tarkowski R, Uliasz-Misiak B. Prospects for the use of carbon dioxide in enhanced geothermal systems in Poland. J Clean Prod 2019;229:1189–1197. https://doi.org/10.1016/j.jclepro.2019.05.036.

[8] Bielicki JM, Leveni M, Johnson JX, Ellis BR. The promise of coupling geologic CO_2 storage with sedimentary basin geothermal power generation.

iScience 2023;26(2):105618. https://doi.org/10.1016/j.isci.2022.105618.
[9] Aminu MD, Nabavi SA, Rochelle CA, Manovic V. A review of developments in carbon dioxide storage. Appl Energy 2017;208:1389-1419. https://doi.org/10.1016/j.apenergy.2017.09.015.
[10] Zhang X, Li L, Da Q, Su Y, Ma S, Zhu Z. Microfluidic investigation on multiphase interaction and flow behavior of immiscible/miscible gases in deep heterogeneous reservoir. J Environ Chem Eng 2022;10(6):109036.
https://doi.org/10.1016/J.JECE.2022.109036.
[11] Al-Zaidi E, Nash J, Fan X. Effect of CO_2 phase on its water displacements in a sandstone core sample. Int J Greenh Gas Con 2018;71:227–238. https://doi.org/10.1016/j.ijggc.2018.01.018.
[12] Basirat F, Yang Z, Niemi A. Pore-scale modeling of wettability effects on CO_2–brine displacement during geological storage. Adv Water Resour 2017;109:181-195. https://doi.org/10.1016/j.advwatres.2017.09.004.
[13] Chen Y, Li Y, Valocchi AJ, Christensen KT. Lattice Boltzmann simulations of liquid CO_2 displacing water in a 2D heterogeneous micromodel at reservoir pressure conditions. J Contam Hydrol 2018;212:14-27. https://doi.org/10.1016/j.jconhyd.2017.09.005.
[14] Moghadasi R, Goodarzi S, Zhang Y, Bijeljic B, Blunt MJ, Niemi A. Pore-scale characterization of residual gas remobilization in CO_2 geological storage. Adv Water Resour 2023;179:104499. https://doi.org/10.1016/j.advwatres.2023.104499.
[15] Moghadasi R, Foroughi S, Basirat F, McDougall SR, Tatomir A, Bijeljic B, Blunt MJ, Niemi A. Pore-Scale determination of residual gas remobilization and critical saturation in geological CO_2 storage: a pore-network modeling approach. Water Resour Res 2023;59(6):e2022WR033686.
https://doi.org/10.1029/2022WR033686.
[16] Raeini AQ, Blunt MJ, Bijeljic B. Direct simulations of two-phase flow on micro-CT images of porous media and upscaling of pore-scale forces. Adv Water Resour 2014;74:116–126.
https://doi.org/10.1016/j.advwatres.2014.08.012.
[17] Raeini AQ, Blunt MJ, Bijeljic B. Modelling two-phase flow in porous media at the pore scale using the volume-of-fluid method. J Comput Phys 2012;231(17):5653–5668. https://doi.org/10.1016/j.jcp.2012.04.011.
[18] Hirt C, Nichols B. Volume of fluid (VOF) method for the dynamics of free boundaries. J Comput Phys 1981;39(1):201–225. https://doi.org/10.1016/0021-9991(81)90145-5.
[19] ANSYS, Inc. ANSYS Fluent Theory Guide. 2023. Release 2023 R1 [Online]. Available: https://ansyshelp.ansys.com.
[20] Dehury R, Chowdhury S, Sangwai JS. Dynamics of hydrogen storage in subsurface saline aquifers: A computational and experimental pore-scale displacement study. Int J Hydrogen Energy 2024;64:817–836. https://doi.org/10.1016/j.ijhydene.2024.05.009.
[21] Brackbill JU, Kothe DB, Zemach C. A continuum method for modeling surface tension. J Comput Phys 1992;100(2):335-354. https://doi.org/10.1016/0021-9991(92)90240-Y.
[22] Chowdhury S, Rakesh M, Medhi S, Shrivastava S, Dehury R, Sangwai JS. Three-Phase Fluid Flow Interaction at Pore Scale during Water- and Surfactant-Alternating Gas (WAG/SAG) Injection Using Carbon Dioxide for Geo-Sequestration and Enhanced Oil Recovery. Energ Fuel 2023;37(7):5270–5290.
https://doi.org/10.1021/acs.energyfuels.2c03982.
[23] Lenormand R, Touboul E, Zarcone C. Numerical models and experiments on immiscible displacements in porous media. J Fluid Mech. 1988;189:165–187. https://doi.org/10.1017/S0022112088000953.
[24] Zhang C, Oostrom M, Wietsma TW, Grate JW, Warner MG. Influence of viscous and capillary forces on immiscible fluid displacement: Pore-scale experimental study in a water-wet micromodel demonstrating viscous and capillary fingering. Energ Fuel 2011;25(8):3493–3505. https://doi.org/10.1021/ef101732k.
[25] Span R, Wagner W. A New Equation of State for Carbon Dioxide Covering the Fluid Region from the Triple-Point Temperature to 1100 K at Pressures up to 800 MPa. J Phys Chem Ref Data 1996;25(6):1509–1596. https://doi.org/10.1063/1.555991
[26] Chow YTF, Maitland GC, Trusler JPM. Interfacial tensions of the (CO_2 + N_2 + H_2O) system at temperatures of (298 to 448) K and pressures up to 40 MPa. Journal of Chemical Thermodynamics 2016:93:392–403. https://doi.org/10.1016/j.jct.2015.08.006.
[27] Iglauer S. CO_2-Water-Rock Wettability: Variability, Influencing Factors, and Implications for CO_2 Geostorage. Acc Chem Res 2017;50(5):1134-1142. https://doi.org/10.1021/acs.accounts.6b00602.
[28] Norouzi M, Yazdi AA, Birjandi AK. A numerical study on Saffman-Taylor instability of immiscible viscoelastic-Newtonian displacement in a Hele-Shaw cell. J Nonnewton Fluid Mech 2018;260:109-119. https://doi.org/10.1016/j.jnnfm.2018.06.007.